Tuning quantum corrections to the conductance in Andreev quantum dots

S. Rodríguez-Pérez, G. C. Duarte-Filho, and A. M. S. Macêdo
Departamento de Física, Laboratório de Física Teórica e Computacional, Universidade Federal de Pernambuco, 50670-901 Recife, PE, Brazil

(Received 30 April 2010; published 29 September 2010)

We study the leading quantum interference correction to the conductance of a ballistic quantum dot connected via barriers of arbitrary transparencies to both a normal-metal lead and a superconducting lead, in the absence of time-reversal symmetry. We find that the sign of the quantum correction can be tuned by the transparencies of the barriers. The validity of our final analytical result is confirmed by independent numerical simulations. We also present a simple and intuitive interpretation of the sign change in terms of an interplay between destructive and constructive interferences of pairs of Feynman paths.

DOI: 10.1103/PhysRevB.82.115453 PACS number(s): 74.45.+c, 73.23.−b, 74.78.Na

I. INTRODUCTION

Coherent hybrid systems composed of a normal metal coupled to a superconductor (NS) have been at the center of much current research in quantum transport. One of the remarkable consequences of the superconducting proximity effect in such systems is the prediction and observation, at subgap energy, of large quantum interference corrections to the dominant classical conductance.[1–3] In this regime, the proximity effect is generated by Andreev reflections, which are elementary scattering processes where incident electrons with energy smaller than the gap of the superconductor are reflected at the NS interface as phase-coherent holes. A striking effect predicted in Ref. 4 is that the leading quantum interference correction (QIC) to the conductance of a disordered quantum wire ideally connected to a normal lead and a superconductor is nonvanishing, even when time-reversal symmetry (TRS) is broken. The same effect was later predicted for an ideal Andreev quantum dot, i.e., a normal ballistic chaotic cavity connected ideally to normal and superconducting leads.[5] Interestingly, albeit both results were obtained by employing random-matrix theory, the negative sign of the correction was explained semiclassically in terms of pairs of Feynman paths interfering destructively. Meanwhile, the use of semiclassical methods based on classical trajectories has become a very active and successful research program[6–10] with the description of NS systems being one of its latest development.[11–14] In Ref. 13 the authors concluded that the sign of the leading QIC to the conductance can be controlled by changing the number of channels in the normal leads or by threading a tiny magnetic flux through the dot.

Since potential barriers are of significant importance in both realistic normal[15] and NS (Refs. 16 and 17) systems it is natural to ask whether the transparency of the barriers can also be used to tune the sign of the leading QIC to the conductance. In this work, we answer this question in the experimentally relevant case of an Andreev quantum dot connected to normal and superconducting leads via potential barriers and in the presence of a weak magnetic field breaking TRS. We find that the answer to the above question is yes and we interpret the result in terms of pairs of interfering Feynman paths, thus making contact with the trajectory-based semiclassical approach. Our results are confirmed by independent numerical simulations. We conclude that the barrier driven sign change is caused by a subtle interplay between constructive and destructive interference processes.

II. SCATTERING APPROACH

We assume that a voltage V is applied to the normal lead and that the superconducting lead is grounded. In order to use a scattering approach we insert two artificial normal leads between the cavity and the contacts, as sketched in Fig. 1. It is considered that there are N_n open scattering channels in both sides of the normal-normal (NN) contact, and N_s open channels between the cavity and the NS contact. There are no open channels in the superconducting lead. The imperfection of the NN (NS) contact is modeled by introducing a potential barrier with transparency Γ_n (Γ_s). The pair potential is assumed to be $\Delta=\Delta_0 e^{i\phi}$ in the superconductor and zero in any other part of the system. We further assume that $|eV| \ll \Delta_0$. In this way, a set of eigenfunctions for each normal lead can be obtained from the Bogoliubov-De Gennes equations so that all scattering matrices are well defined.[18] The combined effect of the potential barrier and the Andreev reflections in the NS interface can be modeled as an effective contact,[18] in which the Andreev reflections occurs with a probability $\Gamma_A \equiv \Gamma_s^2/(2-\Gamma_s)^2$, and the normal reflections with probability $(1-\Gamma_A)$.

In order to profit from the diagrammatical method for averaging over the unitary group,[5] we use a stub parametrization for the construction of the scattering matrix S of the whole system.[19] Our particular choice of parametrization

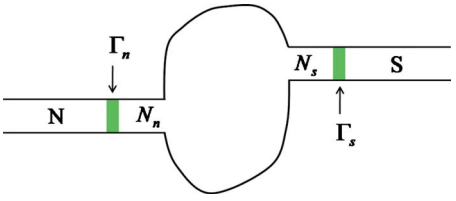

FIG. 1. (Color online) Schematic view of the Andreev quantum dot with broken time-reversal symmetry. The numbers of open channels in each lead are denoted by N_n and N_s while Γ_n and Γ_s are the transparencies of the barriers. The letters N and S denote the normal metal lead and the superconducting lead, respectively.

 ©2010 The American Physical Society

builds on a recent work on ferromagnetic-normal-ferromagnetic systems[20] which is tailor-made for diagrammatic calculations. This parametrization requires the definition of matrices combining the information of the contacts and separating its scattering properties according to the direction of propagation. The transmission properties for quasiparticles leaving the cavity (entering the cavity) are organized in the matrix T' (T). In our model $T=T'$. Denoting $I_{N_{n,s}}$ the $N_{n,s}\times N_{n,s}$ identity matrix, we define

$$T_{\sigma,\sigma';j,j'} = \delta_{\sigma,\sigma'}(\delta_{\sigma,e} + \delta_{\sigma,h}\hat{\mathcal{C}})\delta_{j,j'}\delta_{j,n} i\sqrt{\Gamma_n}\mathrm{I}_{N_n}, \tag{1}$$

where the Greek character σ represents the electron (e)—hole (h) or Nambu degree of freedom, and the indexes j and j' label the terminals. The operation of conjugation is represented by the operator $\hat{\mathcal{C}}$. In a similar way, the reflection amplitudes of the contacts for electrons trying to leave the cavity are organized in the following matrix:

$$R_{\sigma,\sigma';j,j'} = \delta_{j,j'}[\delta_{\sigma,\sigma'}(\delta_{j,s}\sqrt{1-\Gamma_A}\mathrm{I}_{N_s} + \delta_{j,n}\sqrt{1-\Gamma_n}\mathrm{I}_{N_n}) - i(1-\delta_{\sigma,\sigma'})\delta_{j,s}\sqrt{\Gamma_A}\mathrm{I}_{N_s}], \tag{2}$$

while the reflection properties for quasiparticles trying to enter the cavity are expressed through the matrix $\bar{S}$, which is defined as

$$\bar{S}_{\sigma,\sigma';j,j'} = \delta_{\sigma,\sigma'}\delta_{j,j'}\delta_{j,n}\sqrt{1-\Gamma_n}\mathrm{I}_{N_n}. \tag{3}$$

The scattering matrix of the cavity is given by

$$(S_0)_{\sigma,\sigma'} = \delta_{\sigma,\sigma'}(\delta_{\sigma,e} + \delta_{\sigma,h}\hat{\mathcal{C}})U. \tag{4}$$

The matrix U is assumed to be from the circular unitary ensemble.[18] Finally, the scattering matrix of the entire system is given by

$$S = \bar{S} + T'(1 - S_0R)^{-1}S_0T, \tag{5}$$

which is the basic equation of the stub model. A recent alternative scattering approach can be found in Ref. 21.

III. DIAGRAMMATIC CALCULATION

The dimensionless conductance of an NS system at zero temperature is given by[22]

$$G = 2\ \mathrm{tr}[S_{eh}^{nn}(S_{eh}^{nn})^{\dagger}] = 2\ \mathrm{tr}[C^e\delta S C^h \delta S^{\dagger}], \tag{6}$$

where S_{eh}^{nn} is the $N_n\times N_n$ block of the S matrix which contains the probability amplitudes of the process in which an electron comes from the normal lead, enters the cavity, and a hole leaves through the same lead. The matrices $C^{e,h}$ are projectors which extracts the information of S_{eh}^{nn} from the matrix $\delta S = S - \bar{S}$. They are defined as

$$C^{e(h)}_{\sigma,\sigma';j,j'} = \delta_{\sigma,\sigma'}\delta_{\sigma,e(h)}\delta_{j,j'}\delta_{j,n}\mathrm{I}_{N_n}. \tag{7}$$

Substituting Eq. (5) into Eq. (6) and expanding the result in power series we get

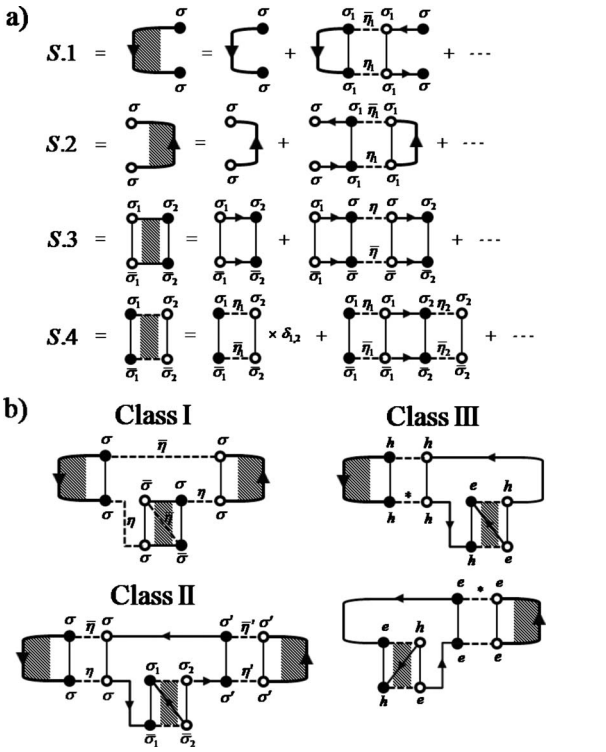

FIG. 2. (a) Diagrammatical definition of four series denoted $S.1$, $S.2$, $S.3$, and $S.4$. (b) Representative sums of crossed diagrams for the three different classes. Einstein summation convention is adopted for Nambu indexes that belong to different T-cycles.

$$G = \sum_{k_1,k_2=0}^{\infty} \mathrm{Tr}[A(S_0R)^{k_1}S_0BS_0^{\dagger}(R^{\dagger}S_0^{\dagger})^{k_2}] \tag{8}$$

in which we defined $A \equiv (T')^{\dagger}C^eT'$ and $B \equiv TC^hT^{\dagger}$. We now average over the unitary ensemble. The average of the terms from Eq. (8) with $k_1=k_2$ yields the "classical" part of the conductance. Diagrammatically, this term is obtained by summing all the ladder diagrams,[5] which we do not present here for brevity. The final result is

$$G_{\mathrm{cl}} = G_nG_A/(G_n + G_A), \tag{9}$$

where $G_n \equiv N_n\Gamma_n$ and $G_A \equiv 2N_s\Gamma_A$. Following Ref. 20 we introduce quantities defined by the infinite series shown in Fig. 2(a), for the calculation of the leading QIC to the conductance. The main difference with respect to Ref. 5 is that each white and black dot is labeled by a Nambu index. Dashed lines represent elements of the diagonal blocks of S_0, and a new symbol denoted by η is introduced to account for the difference between the elements of U^* and U. If $\sigma=e$ $(\sigma=h)$ then η represents the "blank" (asterisk) symbol. The symbol $\bar{\eta}$ represents the opposite of η. Directed lines going from a white (black) dot to a black (white) dot represent blocks of the matrix R $(R^{\dagger})$ while directed lines going from a white (black) dot to a white (black) dot are blocks of the matrix B (A). Thin solid lines represent Kronecker deltas.

The average of the terms in Eq. (8) with $k_1 \neq k_2$ leads to crossed diagrams of the order of unity. Using the series defined in Fig. 2(a), sums of crossed diagrams can be grouped

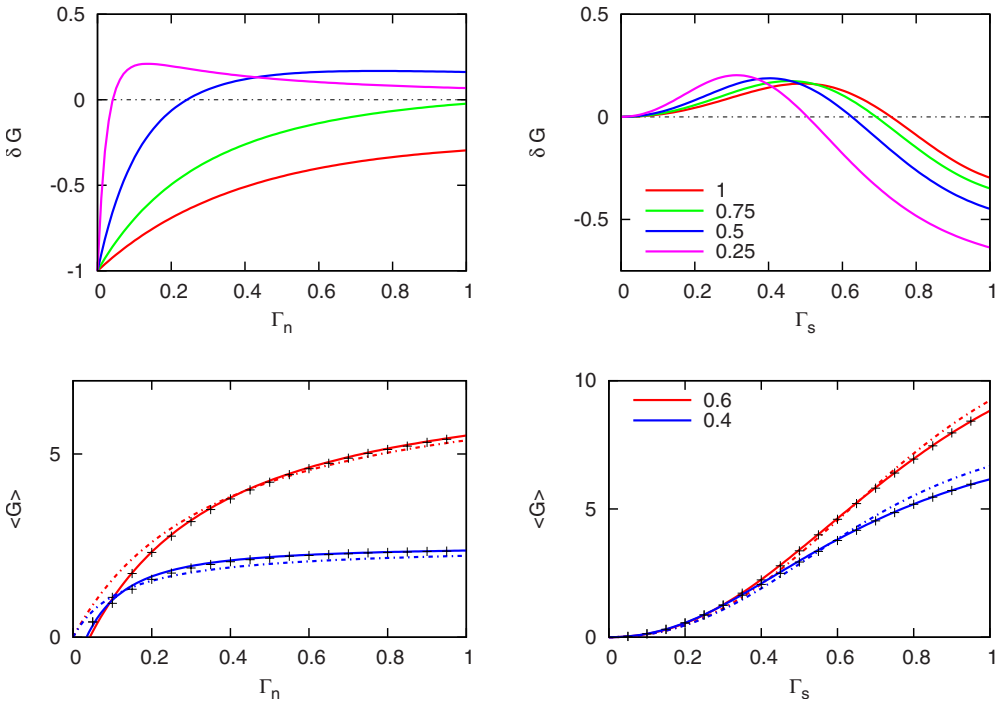

FIG. 3. (Color online) The left (right) panel on the top shows the leading QIC to the conductance as a function of Γ_n (Γ_s), for some fixed values of Γ_s (Γ_n). The dashed line is a guide to the eyes. In the left (right) panel at the bottom we show our analytical results for the average conductance $\langle G\rangle = G_{\rm cl} + \delta G$ (solid lines), the "classical" term $G_{\rm cl}$ (dashed lines), and the conductance calculated via numerical simulations (scatter line).

according to its specific topology, as shown in the Fig. 2(b) for some representative cases. According to the numerical value of each sum, they can be separated into three classes. All diagrams contain two legs, each one going from a black dot, adjacent to a block of A, to a white dot adjacent to a block of B. The leg on the top of the diagram is a chain of blocks of $S_0^\dagger$ and $R^\dagger$, and the leg on the bottom is a chain of blocks of S_0 and R. By inverting the middle part of each diagram represented in Fig. 2(b), the rest of the topologically different diagrams, not represented in the figure, are obtained. They belong to the same class from which they are generated. Summing up all contributions from these crossed diagrams we find the following simple expression for the leading QIC to the conductance:

$$\delta G = -G_A(G_A+G_n)^{-3}[G_A G_n + G_A^2(1-G_n/N_n) - 2G_n^2(1-G_A/N_s)], \tag{10}$$

which is the central result of this paper.

In the left (right) panel on the top of Fig. 3 we plot Eq. (10) as a function of Γ_n (Γ_s) for four fixed values of Γ_s (Γ_n), setting $N_n = N_s$. When Γ_n varies, δG undergoes a sign change if $\Gamma_s > (\sqrt{3}-1)$. By contrast, δG always changes sign and displays a nonmonotonic behavior as a function of Γ_s. Note that if $\Gamma_s \approx 0$ the Andreev reflection processes are suppressed and δG tends to zero, as expected. The panels at the bottom of Fig. 3 show the comparison of our analytical results for $\langle G\rangle = G_{\rm cl} + \delta G$ (solid lines) and $G_{\rm cl}$ (dashed lines) with the average conductance calculated via numerical simulations (scatter line). Note the excellent agreement. In the simulations, we chose $N_n = N_s = 20$ and the average was performed using ensembles of 10^4 random matrices. We stress that the analytical results are valid in the regime $N_s\Gamma_s, N_n\Gamma_n \gg 1$.

IV. SEMICLASSICAL INTERPRETATION

Every crossed diagram can be identified with a type of interfering pair of Feynman paths by associating a specific path to each leg. The series $S.1$ and $S.2$ are always part of both legs in the diagrams, and thus they can be identified with coinciding parts of two paths. More specifically, $S.1$ represents a pair of flights starting with the entry of an electron in the cavity whereas in $S.2$ the flights end with the output of a hole from the cavity. Interference processes are caused by close encounters of noncoinciding parts of the paths, which may occur inside the cavity or at the contacts.[7,13] Let us analyze the three classes separately, using the representative diagrams shown in Fig. 2(b).

A. Class I

Let us focus on the center of the diagram. In the top leg we see that the quasiparticle suffers multiple reflections inside the cavity, which is represented by a dashed line. The central part of the bottom leg is constituted of three dashed lines and $S.3$ with $\sigma_1 = \bar{\sigma}$ and $\sigma_2 = \sigma$. This means that the quasiparticle undergoes $2(2k+1)$ Andreev reflections, where k is an integer. For that reason, the phase difference accumulated in the top and bottom legs is $(2k+1)\pi$, leading to a destructive interference. Mathematically, the destructive interference is expressed by a negative sign coming from the

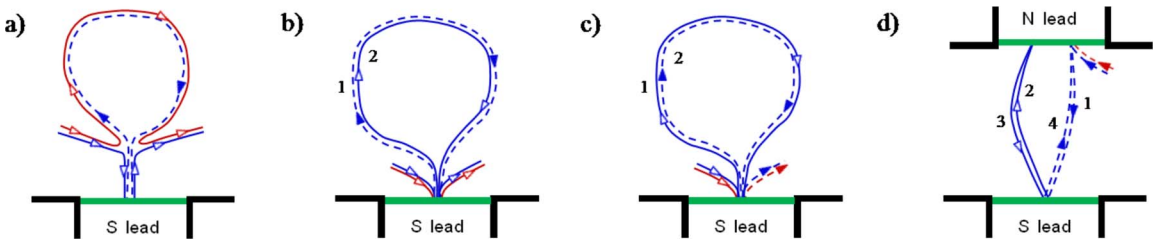

FIG. 4. (Color online) Each colored line identifies one path and the solid (dashed) line represents a quasiparticle traveling like an electron (a hole). The green bars represent the contact of the S and the N leads. The numbers indicates the time order at which the loops are traveled. (a) A simple pair of paths with encounters inside the cavity, typical from Class I. [(b) and (c)] Two pairs of paths with encounters at the NS contact, belonging to the subclasses 1 and 8 of Class II, respectively. (d) A pair of paths with encounter at the NN contact, typical of Class III.

product of the quantities associated with T-cycles. However, there is a U-cycle with four dashed lines in the diagram, whose weight is negative, differently from the U-cycles with two dashed lines which have a positive weight. As a result, the diagram is positive and enhances the conductance. This can be understood in terms of paths that interfere destructively with close encounters inside the cavity. A simple pair of this kind is represented in Fig. 4(a). In Fig. 4 each colored line identifies one path, and the solid (dashed) line represents a quasiparticle traveling like an electron (a hole). The green bars represent the contact of the superconductor with the normal leads. The diagrams of Class I are nonvanishing even when the contacts are ideal.

B. Class II

The noncoinciding part of the paths are determined by one reflection (top leg), and three reflections, and $S.4$ (bottom leg). Note that the reflection associated with the top leg is joined by two Kronecker delta to two reflections indicated in the bottom leg, which implies that they occur in the same contact. The interfering paths have thus their encounters at one of the contacts. Depending on what kind of reflection each member of the above triplet is, which mathematically is expressed by the values that σ_1, σ_2, and σ' can take with respect to σ, we can define eight subclasses of diagrams, shown in Table I. The only subclass whose interfering paths can have their encounters at both contacts is the subclass 2 because all reflections of the triplet are normal. The other subclasses have their encounters at the NS interface. The difference between the phases accumulated in both legs is an even number times π for the subclasses 3 and 8, implying constructive interference. In this way, these two subclasses tend to enhance the conductance. For the other subclasses the interference is destructive and they tend to reduce the conductance. In order to exemplify how both kinds of interference may occur, we show in Figs. 4(b) and 4(c) two simple pairs of paths corresponding to the subclasses 1 and 8, respectively. The numbers on the loops indicate the order of travel time. The signs of the diagrams of the subclasses are represented in the last row of Table I. The sign of the contribution of Class II may change with the values of the transparencies. In the ideal case, just the subclass 4 is nonzero. This is expected, since only in this class the triplet is constituted of Andreev reflections.

C. Class III

In the two representative cases of diagrams shown in Fig. 2(b), the difference between the paths corresponding to top and bottom legs is given by two normal reflections and $S.4$ with $\sigma_1 = e$ and $\sigma_2 = h$ in the bottom leg. Note that both reflections are joined via deltas to a block of A or to a block of B, which means that the encounters take place at the NN contact. For that reason, diagrams of Class III vanish if $\Gamma_n = 1$. Since the accumulated phase in $S.4$ is an odd number times π, if $\sigma_1 \neq \sigma_2$, a destructive interference takes place at the NN contact. Therefore, all diagrams of this class tend to reduce the conductance. A simple pair of paths of this class, corresponding to a process in which two holes leave the cavity by different interfering paths, is shown in Fig. 4(d).

V. CONCLUSIONS

We conclude by observing that the effect predicted in this

TABLE I. Eight subclasses of Class II. The signs of the diagrams of each subclass are represented in the last row.

	Subclasses of Class II							
	1	2	3	4	5	6	7	8
σ_1	σ	$\bar{\sigma}$	σ	σ	$\bar{\sigma}$	$\bar{\sigma}$	σ	$\bar{\sigma}$
σ_2	σ	σ	$\bar{\sigma}$	σ	$\bar{\sigma}$	σ	$\bar{\sigma}$	$\bar{\sigma}$
σ'	σ	σ	σ	$\bar{\sigma}$	σ	$\bar{\sigma}$	$\bar{\sigma}$	$\bar{\sigma}$
Sign	−	−	+	−	−	−	−	+

paper could, in principle, be measured within the current technology of hybrid NS structures, as can be seen in Refs. 16 and 23. In Ref. 23 the conductance of a quantum dot coupled to a normal lead and to a superconducting one has been measured varying a gate voltage which controls the ratio between the tunnel rate of the barriers. In Ref. 16 an SNS system is studied and the model of a chaotic quantum dot with imperfect contacts is found adequate to explain the experimental data.

ACKNOWLEDGMENTS

We would like to thank Philippe Jacquod for many useful remarks. This work was partially supported by CNPq and FACEPE (Brazilian Agencies).

[1] P. C. van Son, H. van Kempen, and P. Wyder, Phys. Rev. Lett. **59**, 2226 (1987).
[2] A. Kastalsky, A. W. Kleinsasser, L. H. Greene, R. Bhat, F. P. Milliken, and J. P. Harbison, Phys. Rev. Lett. **67**, 3026 (1991).
[3] K. M. H. Lenssen, L. A. Westerling, C. J. P. M. Harmans, J. E. Mooij, M. R. Leys, W. van der Vleuten, and J. H. Wolter, Surf. Sci. **305**, 476 (1994).
[4] P. W. Brouwer and C. W. J. Beenakker, Phys. Rev. B **52**, R3868 (1995).
[5] P. W. Brouwer and C. W. J. Beenakker, J. Math. Phys. **37**, 4904 (1996).
[6] K. Richter and M. Sieber, Phys. Rev. Lett. **89**, 206801 (2002).
[7] R. S. Whitney and Ph. Jacquod, Phys. Rev. Lett. **96**, 206804 (2006).
[8] P. Braun, S. Heusler, S. Müller, and F. Haake, J. Phys. A **39**, L159 (2006).
[9] P. W. Brouwer and S. Rahav, Phys. Rev. B **74**, 085313 (2006).
[10] G. Berkolaiko, J. M. Harrison, and M. Novaes, J. Phys. A **41**, 365102 (2008).
[11] M. C. Goorden, Ph. Jacquod, and J. Weiss, Nanotechnology **19**, 135401 (2008).
[12] M. C. Goorden, Ph. Jacquod, and J. Weiss, Phys. Rev. Lett. **100**, 067001 (2008).
[13] R. S. Whitney and Ph. Jacquod, Phys. Rev. Lett. **103**, 247002 (2009).
[14] J. Kuipers, D. Waltner, C. Petitjean, G. Berkolaiko, and K. Richter, Phys. Rev. Lett. **104**, 027001 (2010).
[15] S. Oberholzer, E. V. Sukhorukov, C. Strunk, C. Schönenberger, T. Heinzel, and M. Holland, Phys. Rev. Lett. **86**, 2114 (2001); S. Oberholzer, E. V. Sukhorukov, C. Strunk, and C. Schönenberger, Phys. Rev. B **66**, 233304 (2002).
[16] T. S. Jespersen, M. L. Polianski, C. B. Sorensen, K. Flensberg, and J. Nygard, N. J. Phys. **11**, 113025 (2009).
[17] T. Domański and A. Donabidowicz, Phys. Rev. B **78**, 073105 (2008).
[18] C. W. J. Beenakker, Rev. Mod. Phys. **69**, 731 (1997).
[19] F. Domínguez-Adame, E. Maciá, and A. Sánchez, Phys. Rev. B **51**, 878 (1995).
[20] S. Rodríguez-Pérez, A. L. R. Barbosa, and A. M. S. Macêdo, Phys. Rev. B **81**, 085326 (2010).
[21] V. A. Gopar, J. A. Méndez-Bermúdez, and A. H. Aly, Phys. Rev. B **79**, 245412 (2009).
[22] C. J. Lambert, J. Phys.: Condens. Matter **5**, 707 (1993).
[23] R. S. Deacon, Y. Tanaka, A. Oiwa, R. Sakano, K. Yoshida, K. Shibata, K. Hirakawa, and S. Tarucha, Phys. Rev. Lett. **104**, 076805 (2010); Phys. Rev. B **81**, 121308(R) (2010).